Elastic Spherical Cloak Driven by Bayesian Optimization

Zhiwei Yang(杨志伟)[1,2†], Xiaofan Wang(王笑凡)[1†], Hongbo Xu(徐鸿博)[1], Xiaochao Li(李晓潮)[2*], Shan Zhu(朱杉)[3*], and Huanyang Chen(陈焕阳)[1*]

[1]*Department of Physics, Xiamen University, Xiamen 361005, China*
[2]*Department of Microelectronics and Integrated Circuit, Xiamen University, Xiamen 361005, China*
[3]*Quantum Science Center of Guangdong-Hong Kong-Macao Greater Bay Area (Guangdong), Shenzhen-Hong Kong International Science and Technology Park, Shenzhen 518000, China*

(Received 7 October 2024; accepted manuscript online 9 December 2024)

The introduction of machine learning algorithms has revolutionized the design of invisible devices, particularly in the intricate domain of elasto-dynamics. In this study, we proposed a core-shell configuration to realize elastic sphere cloaks driven by a Bayesian optimization algorithm to pinpoint the optimal configuration with high precision. Numerical simulations in solid and aqueous environments were performed to validate the cloaking efficacy of our design and the parameters identified by the algorithm. The results closely agreed with the theoretical predictions, underscoring the robustness of the proposed method. This approach provides new insights into the design of elastic wave invisibility devices and has potential applications in underwater communication and sonar detection.

DOI: 10.1088/0256-307X/42/1/014302 CSTR: 32039.14.0256-307X.42.1.014302

Invisibility has always been a popular topic in metamaterials research. Transformation optics is a powerful method for achieving invisibility,[1] in which material distributions are designed to guide incident waves around obstacles, thereby avoiding scattering. This method was initially applied to the electromagnetic waves[2] and has since been gradually extended to acoustic,[3–8] thermal,[9–12] and quantum matter waves.[13–15] The most important aspect of transformation optics is the form-invariance of the governing equations under coordinate transformation. However, the elastic wave equation does not satisfy this condition; therefore, achieving an elastic wave cloak using the classical transformation method is not feasible. Nevertheless, linear[16,17] and nonlinear transformation methods[18–21] have been used to approximate the transformation control equations to achieve two-dimensional flexural wave cloaks. However, transformation-based cloaks typically possess complex anisotropic material parameters and uncontrollable operating frequencies. In this context, alternative invisibility technologies have emerged, such as carpet cloaking,[22–24] active cloaking,[25,26] waveguide cloaking,[27,28] and scattering cancellation.[29]

In recent years, cloaks based on acoustic scattering cancellation have attracted considerable attention. Compared to transformation-based methods, scattering cancellation techniques require multiple layers of isotropic materials to achieve near-perfect cloaks, thus increasing the feasibility of invisibility cloaks.[30,31] By adjusting the material parameters and thickness of each layer, the original scattering components can be coherently canceled out by the counter propagating waves produced by the structure, resulting in a near-zero scattering cross section (SCS). However, the introduction of the same method to eliminate scattering in solids poses greater challenges.[32] Owing to the presence of shear forces, acoustic waves in solids (i.e., elastic waves) possess both transverse and longitudinal components, leading to a more complex response between the scattering components and material parameters. Consequently, the manual tuning of material parameters is often time-consuming and arduous, compounded by the challenge of exhaustively exploring the entire parameter space. Hence, researchers are investigating the application of optimization algorithms such as genetic[33] and topology optimization[34] algorithms to determine the necessary parameters. However, their performances showed variability and did not consistently meet expectations. For instance, genetic algorithms frequently converge on local optima, and topology optimization algorithms are often limited to the design of certain types of irregular structures.[35,36] Recently, the integration of deep learning, a subset of artificial intelligence techniques, has demonstrated impressive outcomes.[37–42] Nonetheless, extensive datasets are required to train neural networks, and the fine-tuning of grid hyperparameters to enhance precision is time consuming and can amplify the workload when addressing particular problems. Bayesian optimization algorithms are promising alternatives to conventional optimization techniques and deep learning approaches. Bayesian optimization excels in managing costly or noisy objective functions and efficiently navigates high-dimensional parameter

†These authors contributed equally to this work.
*Corresponding author. Email: leexcjeffrey@xmu.edu.cn; zhushan@quantumsc.cn; kenyon@xmu.edu.cn
© 2025 Chinese Physical Society and IOP Publishing Ltd. All rights, including for text and data mining, AI training, and similar technologies, are reserved.

spaces with fewer evaluations. Unlike genetic algorithms, which explore diverse spaces but may get trapped in local optima, Bayesian optimization balances exploration and exploitation through acquisition functions, thereby enhancing the chances of reaching a global optimum. It is especially advantageous for parameter-intensive tasks such as designing invisibility cloaks, because it rapidly identifies promising regions and reduces computational expense. Compared with topology optimization, it adapts more flexibly to various geometries and materials, and unlike deep learning, it is sample-efficient and better suited for handling uncertainty. Consequently, Bayesian optimization algorithms are inherently well-suited for exploring parameters required to develop elastic invisibility cloaks.

In this study, we utilized the Mie scattering theory to determine the distribution of scattering fields and SCS. A Bayesian optimization algorithm was then used to explore the parameter space and extract the geometric and material parameters that can achieve a near-zero SCS. In the first case, we designed a single-layer cloak for an elastic sphere in a solid environment with longitudinal wave incidence. The numerical simulation results were consistent with the theoretical predictions, demonstrating the excellent performance of the method. Furthermore, we investigated a case with tangible practical implications: the perfect invisibility of an elastic sphere in an aqueous environment. As water is a commonly encountered liquid medium, its utilization as the host medium to achieve invisibility of acoustic and elastic waves will have potential applications in underwater communication and sonar detection scenarios.

We consider a three-dimensional elastic cloaking problem. We aim to conceal an elastic spherical scatter with radius r_1 mass density ρ_1, and Lamé coefficients λ_1 and μ_1, represented by the red core sphere in Fig. 1(a), from a host medium with materials parameters (ρ_3, λ_3, μ_3). To achieve this objective, we proposed a shell cloak with radius r_2 and material parameters (ρ_2, λ_2, μ_2). We assumed that a plane longitudinal wave propagating along the x-axis was the incident wave on the designed structure [Fig. 1(b)]. The incident and resulting waves in each domain can be expressed by the Rayleigh expansion of the scalar potentials, as follows:

$$\phi_{\rm inc} = \phi_0 \mathrm{e}^{-\mathrm{i}\omega t} \sum i^n (2n+1) J_n(k_{d1} r) P_n(\cos\theta), \tag{1}$$

$$\phi_3 = \phi_0 \mathrm{e}^{-\mathrm{i}\omega t} \sum i^n (2n+1) a_n H_n(k_{d1} r) P_n(\cos\theta), \tag{2}$$

$$\chi_3 = \phi_0 \mathrm{e}^{-\mathrm{i}\omega t} \sum i^n (2n+1) b_n H_n(k_{s1} r) P_n(\cos\theta), \tag{3}$$

$$\phi_2 = \phi_0 \mathrm{e}^{-\mathrm{i}\omega t} \sum i^n (2n+1) [c_n J_n(k_{d2} r) + d_n Y_n(k_{d2} r)] P_n(\cos\theta), \tag{4}$$

$$\chi_2 = \phi_0 \mathrm{e}^{-\mathrm{i}\omega t} \sum i^n (2n+1) [e_n J_n(k_{s2} r) + f_n Y_n(k_{s2} r)] P_n(\cos\theta), \tag{5}$$

$$\phi_1 = \phi_0 \mathrm{e}^{-\mathrm{i}\omega t} \sum i^n (2n+1) g_n J_n(k_{d2} r) P_n(\cos\theta), \tag{6}$$

$$\chi_1 = \phi_0 \mathrm{e}^{-\mathrm{i}\omega t} \sum i^n (2n+1) h_n J_n(k_{s2} r) P_n(\cos\theta), \tag{7}$$

$$k_{dn} = \frac{\omega}{v_l},\ v_l = \sqrt{\frac{(\lambda+2\mu)}{\rho}},\ k_{sn} = \frac{\omega}{v_t},\ v_t = \sqrt{\frac{\mu}{\rho}}. \tag{8}$$

Here, $\phi_{\rm inc}$ is the scalar potential of incident wave, and ϕ_1, ϕ_2, ϕ_3 and χ_1, χ_2, χ_3 are the scalar potentials of the longitudinal and shear waves of the cloaked region, cloaking region, and host medium, respectively. ϕ_0 is the amplitude factor; ω is the angular frequency; $J_n(x)$ and $Y_n(x)$ are the nth order first and second kind of spherical Bessel function; $H_n(x)$ is the nth order first kind of spherical Hankel function; $P_n(z)$ is the nth order Legendre function; $k_{dn}(k_{sn})$ is the longitudinal (transverse) wave number in the nth substrate; and a_n and h_n are the coefficients to be determined. By applying the boundary conditions, we obtain the following matrix equation (see Ref. [43] for detailed expressions of the matrix elements).

$$\begin{bmatrix} d_{11}^{(n)} & d_{12}^{(n)} & d_{13}^{(n)} & d_{14}^{(n)} & d_{15}^{(n)} & d_{16}^{(n)} & d_{17}^{(n)} & d_{18}^{(n)} \\ d_{21}^{(n)} & d_{22}^{(n)} & d_{23}^{(n)} & d_{24}^{(n)} & d_{25}^{(n)} & d_{26}^{(n)} & d_{27}^{(n)} & d_{28}^{(n)} \\ d_{31}^{(n)} & d_{32}^{(n)} & d_{33}^{(n)} & d_{34}^{(n)} & d_{35}^{(n)} & d_{36}^{(n)} & d_{37}^{(n)} & d_{38}^{(n)} \\ d_{41}^{(n)} & d_{42}^{(n)} & d_{43}^{(n)} & d_{44}^{(n)} & d_{45}^{(n)} & d_{46}^{(n)} & d_{47}^{(n)} & d_{48}^{(n)} \\ d_{51}^{(n)} & d_{52}^{(n)} & d_{53}^{(n)} & d_{54}^{(n)} & d_{55}^{(n)} & d_{56}^{(n)} & d_{57}^{(n)} & d_{58}^{(n)} \\ d_{61}^{(n)} & d_{62}^{(n)} & d_{63}^{(n)} & d_{64}^{(n)} & d_{65}^{(n)} & d_{66}^{(n)} & d_{67}^{(n)} & d_{68}^{(n)} \\ d_{71}^{(n)} & d_{72}^{(n)} & d_{73}^{(n)} & d_{74}^{(n)} & d_{75}^{(n)} & d_{76}^{(n)} & d_{77}^{(n)} & d_{78}^{(n)} \\ d_{81}^{(n)} & d_{82}^{(n)} & d_{83}^{(n)} & d_{84}^{(n)} & d_{85}^{(n)} & d_{86}^{(n)} & d_{87}^{(n)} & d_{88}^{(n)} \end{bmatrix} \begin{bmatrix} a_n \\ b_n \\ c_n \\ d_n \\ e_n \\ f_n \\ g_n \\ h_n \end{bmatrix} = \begin{bmatrix} r_1^{(n)} \\ r_2^{(n)} \\ r_3^{(n)} \\ r_4^{(n)} \\ r_5^{(n)} \\ r_6^{(n)} \\ r_7^{(n)} \\ r_8^{(n)} \end{bmatrix}. \tag{9}$$

To achieve invisibility in different scenarios, the SCS of the entire system must be approximately zero at a certain operating frequency. For a solid medium, SCS is related to a_n and b_n because both longitudinal and shear waves exist. A fluid medium supports only longitudinal waves; therefore, only a_n is required to obtain the SCS. The values of a_n and b_n were calculated by solving the above matrix equation, and subsequently the exact conditions to achieve a near-zero SCS were determined. Here, we constructed a parameter space that included the geometric and material parameters (r_n, ρ_n, λ_n, μ_n) of each region and the wavelength of the incident wave λ to determine the required condition. Bayesian optimization was utilized to expedite this process. The Bayesian optimization process [Fig. 1(c)] starts with a random population of cloak designs and then uses a Gaussian regression process to fit the SCS. The Gaussian regression process begins by initializing the surrogate model (which is used to model the objective function), and the acquisition function (which determines the location of the next sampling point) iteratively fits the sur-

rogate model until the criteria are reached. The aforementioned variables form a one-dimensional array to ensure the Bayesian optimization process.

We demonstrate the effectiveness of our method by providing two examples. First, we considered the case of a solid host medium. We set the mass density ρ_0 and bulk modulus of water λ_0 to 998 kg/m and 2.19 Gpa, respectively, at room temperature. The material properties of all materials, including solid media, are relative to those of water. The material properties of the host medium (ρ_3, λ_3, μ_3), cloaking layer (r_2, ρ_2, λ_2, μ_2), spherical scattering obstacle (r_1, ρ_1, λ_1, μ_1), and wavelength of the incident wave λ were set as parameters to be optimized. In this case, the SCS of the entire system is given by:

$$\sigma_{\text{scs}} = \frac{4\pi}{(k_1)^2}\sum_{l=0}^{\infty}(2l+1)(a_n)^2 + \frac{4\pi}{(k_1)^2}\frac{k_1}{k_2}\sum_{l=0}^{\infty} l(l+1)(2l+1)(b_n)^2, \quad (10)$$

where a_n and b_n represent the coefficients of scattering of longitudinal and transverse waves, respectively, and $k_1(k_2)$ is the wave number of the longitudinal (transverse) waves in the host medium. The optimal ranges of each variable are listed in Table 1. In contrast to the conventional approach, where the operating wavelength is typically much larger than the scale of the invisibility region, the dimensions of the cloaking region designed in this study were comparable to the wavelength, effectively expanding the cloaking coverage. Consequently, the design parameter range of r_1 was matched with the wavelength range. In addition, considering the material parameters of common natural materials such as aluminum ($\rho = 2700\,\text{kg/m}^3$, $\lambda = 51\,\text{Gpa}$, $\mu = 26\,\text{Gpa}$), copper ($\rho = 8960\,\text{kg/m}^3$, $\lambda = 120\,\text{Gpa}$, $\mu = 46\,\text{Gpa}$) and glass ($\rho = 2500\,\text{kg/m}^3$, $\lambda = 30\,\text{Gpa}$, $\mu = 26\,\text{Gpa}$), we set the design range for the mass density and Lamé coefficients of material of each layer as shown in Table 1. Using the Bayesian algorithm for optimization, the relationship between the SCS and number of iterations (black line) is shown in Fig. 1(d). After 190 iterations, the SCS reaches a minimum value of 0.0207. The series of optimized parameters obtained are listed in Table 1. In the parameter space for optimization, both cases may have multiple optimal solutions. Here, we considered water as an example (for details, please refer to the Supplementary Materials).

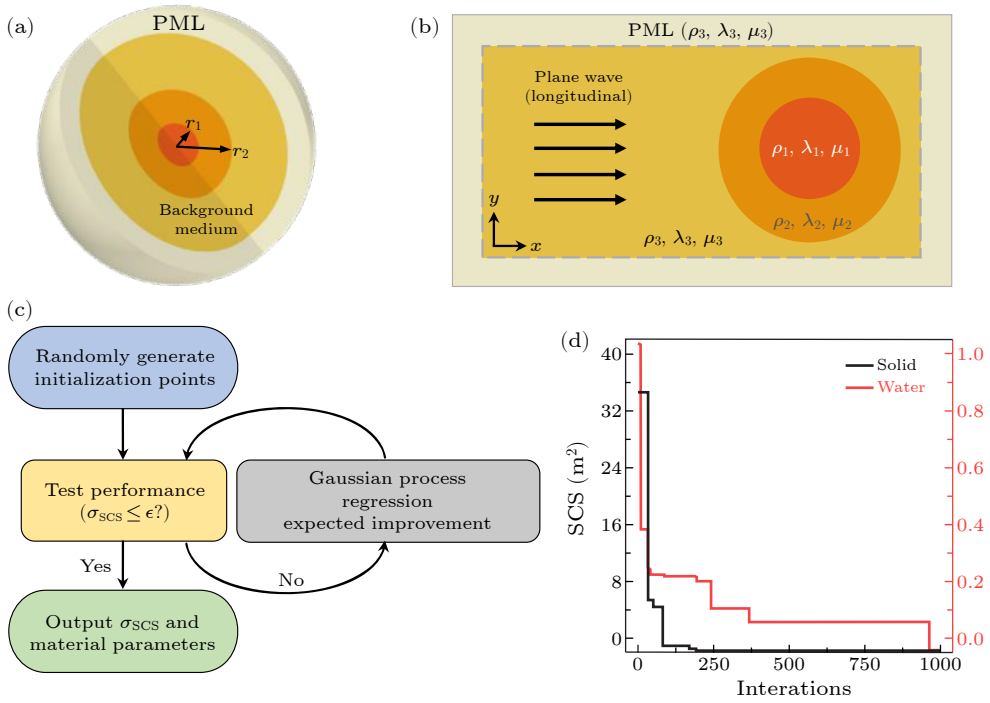

Fig. 1. (a) Schematic for the design of a double layer invisibility cloak. (b) The incident plane wave (longitudinal) has an operating wavelength of λ. The properties of the background material, cloaking layer, spherical scatter, ρ_n, λ_n, μ_n (where $n = 1, 2, 3$ is the layer index), and the radius r are the variables to be optimized. (c) Bayesian optimization framework diagram used here. (d) Iterative graph of SCS for different host media. The black and red lines indicate solid and water as host media, respectively.

Table 1. Optimization range of each variable when the host medium is solid.

Parameter	λ	r_1	r_2	ρ_1/ρ_0	ρ_2/ρ_0	ρ_3/ρ_0	λ_1/λ_0	λ_2/λ_0	λ_3/λ_0	μ_1/λ_0	μ_2/λ_0	μ_3/λ_0
Range	(1, 8)	(1, 8)	(0.2, 6)	(0.5, 22)	(0.5, 26)	(0.5, 19)	(5, 15)	(4, 15)	(4, 15)	(8, 15)	(7, 15)	(6, 15)

Table 2. Optimized material properties of the objects to be cloaked and the corresponding cloaking layer, when the host medium is solid, relative to the water.

Parameter	λ	r_1	r_2	ρ_1/ρ_0	ρ_2/ρ_0	ρ_3/ρ_0	λ_1/λ_0	λ_2/λ_0	λ_3/λ_0	μ_1/λ_0	μ_2/λ_0	μ_3/λ_0
Value	3.847	3.000	3.993	17.888	16.325	14.497	7.525	6.888	6.033	10.314	9.432	8.289

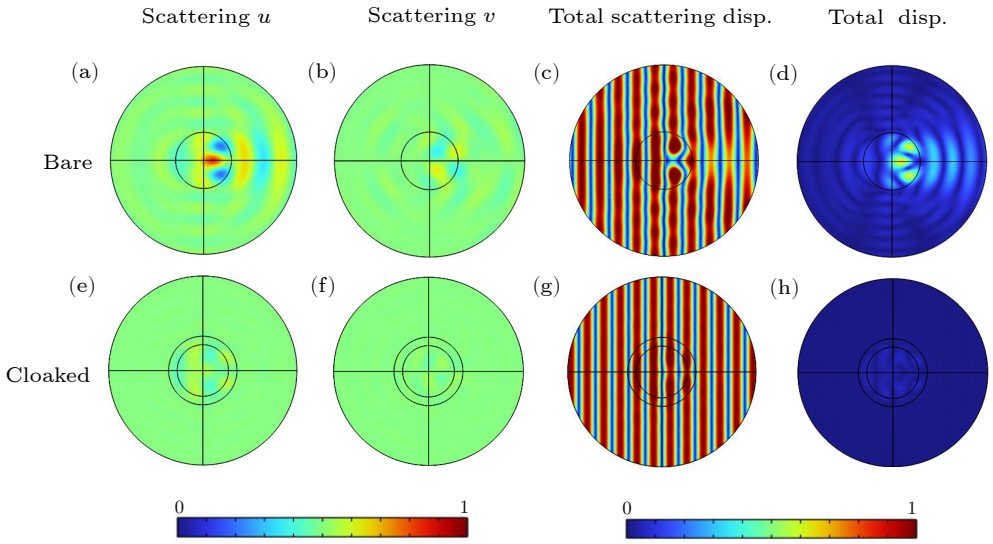

Fig. 2. Numerical simulations for the designed solid cloak. (a)–(d) Scattering u, v, total displacement field, and total scattering fields produced by an incident plane wave for the bare object and (e)–(h) cloaking object.

Table 3. Optimization range of each variable when water is used as medium.

Parameter	λ	r_1	r_2	ρ_1/ρ_0	ρ_2/ρ_0	λ_1/λ_0	λ_2/λ_0	μ_1/λ_0	μ_2/λ_0
Range	(1, 8)	(1, 8)	(0.2, 6)	(0.5, 22)	(0.5, 26)	(1.5, 15)	(1.5, 15)	(0.8, 15)	(7, 15)

Table 4. Optimized material properties of objects to be cloaked and the corresponding cloaking layers, relative to those of water. The background material is water.

Parameter	λ	r_1	r_2	ρ_1/ρ_0	ρ_2/ρ_0	λ_1/λ_0	λ_2/λ_0	μ_1/λ_0	μ_2/λ_0
Value	7.24	4.093	5.708	5.317	20.577	2.055	2.198	1.27	11.768

To verify the performance of the designed invisibility cloak, we used the predicted parameters to conduct three-dimensional (3D) full-wave simulations using COMSOL Multiphysics, and the results are illustrated in Figs. 2(a)–2(h). Figures 2(a) and 2(b), 2(e) and 2(f) depict the scattering fields u and v produced by the bare and cloaking objects under plane wave incidence. Figure 2(a) shows that the entire wave is distorted under the incidence of a plane wave on a bare object, indicating strong scattering. In contrast, the field distribution of the cloaked object is minimally affected. To visually compare the cloaking effects, the total sound pressure field and total scattering displacement field are presented in Figs. 2(c) and 2(d), 2(g) and 2(h), respectively. In the absence of the cloaking layer, the elastic sphere undergoes a strong scattering of sound waves. However, with the cloaking layer, the scattering decreases dramatically. To explore the impact of the cloaking-layer parameters on the SCS, we separately analyzed the two cases (see the Supplementary Materials for details).

We now consider an elastic sphere immersed in water. Because water is non-viscous, μ is zero. The dimensions of Eq. (9) can be reduced from 8×8 to 7×7: In this case, only the longitudinal wave component exists in the scattered waves; hence, the SCS of the entire system is

$$\sigma_{\mathrm{scs}} = \frac{4\pi}{(k_1)^2} \sum_{l=0}^{\infty} (2l+1)(a_n)^2. \tag{11}$$

Combining the Bayesian optimization algorithm with the variables to be optimized and iterate. The difference with the first case is that the variables to be optimized include only the material information of the cloaking layer and elastic sphere. The optimal range of each variable is shown in Table 3. The relationship between the SCS and number of iterations [red line in Fig. 1(d)] was obtained by combining the variable optimization range and Bayesian algorithm for optimization. After 1000 iterations, the SCS reached a minimum value of 0.0446. The series of optimized parameters obtained are listed in Table 4.

To verify the performance of the designed cloak, we conducted full-wave simulations using COMSOL, and the results are shown in Fig. 3. To accurately demonstrate the cloaking effect, we define $\sigma_{\mathrm{R}} = 20 \times \log 10(\sigma_{\mathrm{cloak}}/\sigma_{\mathrm{bare}})$, and the relationship between σ_{R} and the wavelength is shown in Fig. 3(a). The results clearly indicate that resonance occurs when the wavelength is equal to 7.17 m, and the blue region indicates that the working wavelength ranges are 6.9–7.13 m and 7.2–7.42 m. Cloaking was satisfactory when $\sigma_{\mathrm{R}} < 75$ dB. Figures 3(b)–3(d) further depict the total and the scattering fields corresponding to the bare and cloaking objects under the incident plane waves. These figures show the distortion of the entire wave under the incidence of a plane wave on a bare object, indicating strong scattering. In contrast, the field distribution of the invisible object is hardly affected, demonstrating perfect cloaking performance.

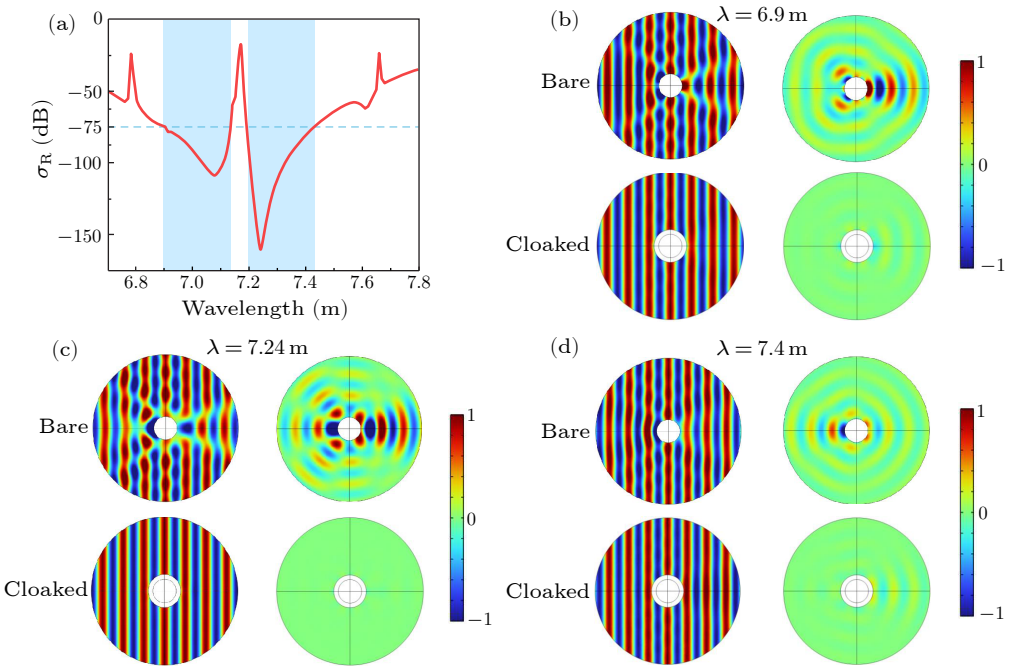

Fig. 3. Numerical simulations for the designed solid cloak. (a) Relation between the SCS and wavelength, when the host medium is water. (b)–(d) Total pressure and scattering field distribution produced by an incident plane wave for the bare and cloaked objects.

The two aforementioned examples have limitations, particularly with respect to the working frequency band and material parameter selection. In practice, broad frequency bands are desirable. However, achieving broadband invisibility may require additional layers, which increase both design complexity and cost. Therefore, the performance and cost must be balanced. The designed material parameters may not occur naturally; however, metamaterials can be used to resolve this issue. Although the combination of these two technologies makes the realization of broadband invisibility cloaks feasible, fabricating such broadband cloaks requires appropriate manufacturing techniques. A practical approach for fabricating broadband elastic cloaks involves multi material additive manufacturing, which enables precise control over the material distribution in each layer to achieve the required Lamé parameters and density values. In addition to the production of materials, the shape of the corresponding invisible spherical cloak is crucial. Three-dimensional printing, which is an advanced manufacturing technology that creates three-dimensional objects layer by layer from digital designs, can solve this problem. Ultimately, combining 3D printing technology with these materials could facilitate the practical realization of theoretical designs of invisible cloaks.

In summary, we proposed and designed a machine-learning-driven single cloaking layer structure for elastic spherical invisibility cloaks placed in both solid and water media. In particular, we employed a Bayesian optimization algorithm for the inverse design of invisibility cloaks, because it required only a few samples to determine the global optimum in high-dimensional spaces and thus avoided the time-consuming post-processing of generated designs. The parameters designed by the Bayesian optimization algorithm can achieve perfect invisibility at multiple frequency points and are applicable to the design of invisibility for larger targets, particularly when the host medium is water. The cloaking frequency band comprised two sections: 197.5–206.3 Hz and 207.7–214.67 Hz. Thus, the combination of artificial intelligence and elastic wave theory serves as a promising and versatile platform for designing outstanding invisibility phenomena. However, our method is only suitable for spheres, whose SCS can be analytically derived. For arbitrarily shaped objects in a solid, the SCS cannot be analytically determined; thus, our method cannot be extended to such objects in a solid medium. We envisage that this approach can be widely used to automate complex material system design processes with minimal human intervention.

Acknowledgements. This work was supported by the National Key Research and Development Program of China (Grant Nos. 2023YFA1407100 and 2020YFA0710100) and the National Natural Science Foundation of China (Grant Nos. 12374410 and 12361161667).

References

[1] Leonhardt U 2006 *Science* **312** 1777
[2] Pendry J B, Schurig D, and Smith D R 2006 *Science* **312** 1780
[3] Milton G W, Briane M and Willis J R 2006 *New J. Phys.* **8** 248
[4] Cummer S A and Schurig D 2007 *New J. Phys.* **9** 45
[5] Chen H and Chan C T 2007 *Appl. Phys. Lett.* **91** 183518
[6] Cummer S A, Popa B I, Schurig D, Smith D R, Pendry J, Rahm M, and Starr A 2008 *Phys. Rev. Lett.* **100** 024301

[7] Zhu X, Liang B, Kan W, Zou X, and Cheng J 2011 *Phys. Rev. Lett.* **106** 014301
[8] Zhu X, Ramezani H, Shi C, Zhu J, and Zhang X 2014 *Phys. Rev. X* **4** 031042
[9] Guenneau S, Amra C, and Veynante D 2012 *Opt. Express* **20** 8207
[10] Li J Y, Gao Y, and Huang J P 2010 *J. Appl. Phys.* **108** 074504
[11] Chen T, Weng C N, and Chen J S 2008 *Appl. Phys. Lett.* **93** 114103
[12] Hu C, Yin Y, and Chen H 2022 *Phys. Rev. Appl.* **18** 024049
[13] Zhang S, Genov D A, Sun C, and Zhang X 2008 *Phys. Rev. Lett.* **100** 123002
[14] Greenleaf A, Kurylev Y, Lassas M, and Uhlmann G 2008 *Phys. Rev. Lett.* **101** 220404
[15] Lin D H 2011 *Phys. Rev. A* **84** 033624
[16] Farhat M, Guenneau S, and Enoch S 2009 *Phys. Rev. Lett.* **103** 024301
[17] Stenger N, Wilhelm M, and Wegener M 2012 *Phys. Rev. Lett.* **108** 014301
[18] Darabi A, Zareei A, Alam M R, and Leamy M J 2018 *Phys. Rev. Lett.* **121** 174301
[19] Liu M and Zhu W D 2019 *J. Sound Vib.* **445** 270
[20] Zareei A and Alam M R 2017 *Phys. Rev. E* **95** 063002
[21] Diatta A and Guenneau S 2014 *Appl. Phys. Lett.* **105** 021901
[22] Li J and Pendry J B 2008 *Phys. Rev. Lett.* **101** 203901
[23] Liu R, Ji C, Mock J J, Chin J Y, Cui T J, and Smith D R 2009 *Science* **323** 366
[24] Valentine J, Li J, Zentgraf T, Bartal G, and Zhang X 2009 *Nat. Mater.* **8** 568
[25] Miller D A B 2006 *Opt. Express* **14** 12457
[26] Greenleaf A, Kurylev Y, Lassas M, and Uhlmann G 2007 *Commun. Math. Phys.* **275** 749
[27] Hu C J, Zeng Y L, Liu Y N, and Chen H Y 2020 *Chin. Phys. Lett.* **37** 054302
[28] Wang X, Chen H, Yin Y, Ruan Y, Zhu S, Hu C, and Chen H 2023 *Adv. Eng. Mater.* **25** 2300025
[29] Alù A and Engheta N 2005 *Phys. Rev. E* **72** 016623
[30] Chen P Y, Farhat M, Guenneau S, Enoch S, and Alù A 2011 *Appl. Phys. Lett.* **99** 191913
[31] Guild M D, Haberman M R, and Alù A 2011 *Wave Motion* **48** 468
[32] Quadrelli D E, Craster R, Kadic M, and Braghin F 2021 *Mech. Lett.* **44** 101262
[33] Mathew T V 2012 *Rep. Submitt. IIT Bombay* **53**
[34] Bendsoe M P and Sigmund O 2013 *Topology Optimization* (Springer Science & Business Media)
[35] Lan L, Sun F, Liu Y, Ong C K, and Ma Y 2013 *Appl. Phys. Lett.* **103** 121113
[36] Fujii G and Akimoto Y 2022 *Opt. Express* **30** 6090
[37] Qian C and Chen H 2021 *Appl. Phys. Lett.* **118** 180501
[38] Qian C, Zheng B, Shen Y, Jing L, Li E, Shen L, and Chen H 2020 *Nat. Photonics* **14** 383
[39] Ahmed W W, Farhat M, Zhang X, and Wu Y 2021 *Phys. Rev. Res.* **3** 013142
[40] Zhen Z, Qian C, Jia Y, Fan Z, Hao R, Cai T, Zheng B, Chen H, and Li E 2021 *Photonics Res.* **9** B229
[41] Luo J, Li X, Zhang X, Guo J, Liu W, Lai Y, Zhan Y, and Huang M 2021 *Opt. Express* **29** 10527
[42] Zhuo L and Amirkulova F 2021 *Congr. Conf. Proc.* **263** 3511
[43] Baird A M, Kerr F H, and Townend D J 1999 *J. Acoust. Soc. Am.* **105** 1527